Electrochemical sensor for luteolin detection

Guosheng Liang[1], Yan Xiao[2], Qiaoling Jing[1], Tingfan Tang[1], Jun Feng[3] and Hao Cheng [1,4]

Abstract

This study developed an electrochemical sensor based on a nitrogen-doped hollow carbon sphere @ZIF-8 composite material (NC@ZIF-8), designed to efficiently detect the natural flavonoid luteolin. The composite material combines the high conductivity of hollow carbon spheres with the large specific surface area of ZIF-8. By optimizing the synthesis process and electrode modification conditions, the sensitivity and selectivity of the sensor were significantly enhanced. Experimental results show that the sensor exhibits excellent detection performance over a wide linear range (0.05–30 μM), with a detection limit as low as 0.011 μM. It also demonstrates good interference resistance and stability. The recovery rates for actual samples (Honeysuckle extract and watermelon juice) ranged from 95.41% to 101.20%, confirming its practical value in food safety and drug analysis.

Introduction

In the modern food industry and in medicine, there is a growing demand for the detection and analysis of natural compounds. Luteolin (3,4,5,7-tetrahydroxy-alone) is a natural flavonoid, widely distributed in plants and fruits, such as celery, oranges, apples, etc.[1]. Luteolin is a natural drug with many pharmacological activities, including uric acid-lowering, antibacterial, antitumor, anti-inflammatory, etc. In the food industry, it is regarded as an important food additive due to its good antioxidant and anti-inflammatory properties, which are used to improve the nutritional value and extend the shelf life of food.

In order to detect luteolin levels in food, it is important to develop a rapid, accurate, and convenient detection method. At present, the main detection methods for luteolin are high-performance liquid chromatography[2], ultraviolet-visible spectrophotometer[3], capillary electrophoresis[4], etc. Although these methods are highly accurate, the disadvantages of expensive instruments, complex operation, and long detection time also make the detection of luteolin costly. In recent years, electrochemistry has entered the field of vision due to its advantages of simple equipment, simple operation, low cost, high reliability, and fast response speed, and it is considered to be an ideal alternative method[5].

Metal–organic frameworks (MOFs) possess unique structural features, including a large specific surface area and tunable pore size and functionality, as well as diverse chemical properties, which endow them with great potential in fields such as catalysis, adsorption, separation, and sensing[6]. Owing to their simple processing and improved electrochemical performance, MOFs are extensively utilized in the fabrication of electrochemical sensors[7]. In particular, ZIF-8, a Zn-based MOF material, has been widely applied in gas storage, separation, catalysis, and electrochemical sensing owing to its unique properties and mild synthesis conditions[8]. When metals are incorporated into MOF-derived carbon materials, they inherit the excellent performance of MOF-derived carbons while retaining their catalytic activity[9]. This combination improves the dispersion of the dual components and enhances selectivity.

As an advanced nanomaterial,N-doped hollow carbon spheres (N-CSSs) combine the high conductivity and chemical stability of carbon materials by introducing nitrogen atoms into carbon spheres to form special doped carbon materials[10]. The large-scale preparation of these materials usually adopts the hard template method, using silicon dioxide (SiO2) as a template,coated with dopamine hydrochloride, and then carbonized at high temperature in a tube furnace to form carbon balls, forming hollow carbon balls by etching templates, and then uniformly

Correspondence: Hao Cheng (iamchenghao@126.com)
[1]Guangxi Key Laboratory of Green Processing of Sugar Resources, College of Biological and Chemical Engineering, Guangxi-University of Science and-Technology, Liuzhou, Guangxi, PR China
[2]GRG Metrology & Test (Nanning) Co., Ltd, Nanning, Guangxi, PR China
Full list of author information is available at the end of the article

growing ZIF-8 inside and outside the carbon balls by in-situ growth method, which effectively avoids the problem of crystal aggregation.

In this study, we developed a composite carbon nanomaterial (NC@ZIF-8) based on nitrogen-doped hollow carbon spheres and ZIF-8 for the preparation of electrochemical sensors for the detection of luteolin. This material exhibits excellent detection performance due to its high specific surface area, high conductivity, and abundant active sites. We describe in detail the synthesis and characterization process of materials, as well as the preparation and optimization methods of electrochemical sensors. The experimental results showed that the NC@ZIF-8/GCE sensor had good recovery and stability in the actual sample detection, which provided an effective method for the rapid and accurate detection of luteolin.

In addition, we conducted a comprehensive evaluation of the electrochemical propertiesof NC@ZIF-8 composites, including cyclic voltammetry (CV), chronocoulometric (CC), current-time curve (I-T), and differential pulse voltammetry (DPV). With these methods, we have optimized the detection conditions and improved the sensitivity and accuracy of the detection. We also investigated the anti-interference capability of the material,demonstrating that the NC@ZIF-8/GCE sensor can accurately and reliably detect luteolin in the presence of multiple potential interfering substances in real-world sample detection.

Finally, we verified the practical application capability of the NC@ZIF-8/GCE sensor in honeysuckle extract and watermelon juice by the standard addition method.

The results showed that the sensor had excellent repeatability and reproducibility, with recoveries ranging from 95.41% to 101.20%, proving its effectiveness and reliability in actual sample detection. These results not only demonstrate the application potential of NC@ZIF-8 composites in the field of electrochemical sensors but also provide a scientific basis for practical applications in the fields of food safety testing and pharmaceutical analysis in the future.

Experimental section
Materials
Ethanol (98%), deionized water, ammonia, tetraethyl silicate (98%, Purchased from Shanghai McLean Biochemical Technology Co., Ltd), dopamine hydrochloride (98%; Purchased from Shanghai McLean Biochemical Technology Co., Ltd), sodium hydroxide (NaOH, analytically pure), 2-methylimidazole (Purchased from Shanghai McLean Biochemical Technology Co., Ltd), zinc nitrate hexahydrate ($Zn(NO_3)_2·6H_2O$), triethylamine, isopropanol (analytically pure), and 5% Nafion were used in this study.

Phosphate buffered saline (PBS, 0.1 M) was prepared from Na_2HPO_4 and NaH_2PO_4, and the pH was adjusted using H_3PO_4 and KOH. All reagents were used as received, without further purification, and all solutions were prepared using ultrapure water.

Synthesis of hollow carbon spheres
First, a mixed solution of ethanol (300 mL), deionized water (90 mL), and ammonia (15 mL) was stirred at room temperature for 30 min. Then, tetraethyl silicate (15 mL) was added to the above solution, and the resulting mixture was stirred vigorously for 1 h, during which silica particles were formed. Thereafter, dopamine hydrochloride (1.5 g) was added to the silica particle suspension, and the resulting mixture was stirred for 12 h. The final product was centrifuged and dried.

The product obtained from the previous reaction was placed in a tube furnace and heated to 900 °C at 3 °C/min and maintained there for 3 h. Then, the carbonized product was placed in a 4 M NaOH solution, and silica was etched away over 24 h to obtain N-doped hollow carbon spheres.

Synthesis of NC@ZIF-8
N-doped hollow carbon spheres (0.3 g) and 2-methylimidazole (0.06 g) were placed in a 50 mL round-bottom flask. Then, deionized water (25 mL) and ethanol (25 mL) were added, the reactants were ultrasonically dispersed, and the mixture was subjected to rotary evaporation for 1.5 h. Thereafter, zinc nitrate (0.06 g) and deionized water (3 mL) were added to the flask, and the contents were again subjected to rotary evaporation for 2 h, and triethylamine (100 μL) was added. The mixture was heated in a water bath at 60 °C for 6 h to evaporate the solvent, and the product was collected by centrifugation, washed with ethanol and water, and dried to obtain NC@ZIF-8. The preparation method of the composite material and the assembly detection of its sensor are shown in Fig. 1.

Preparation of NC@ZIF-8/GCE
Bare GCE was polished with α-Al2O3 powder (0.05 μm), rinsed with ultrapure water and ethanol, and finally dried with nitrogen. Then, an appropriate amount of NC@ZIF-8 was taken in a 10 mL centrifuge tube, measured volumes of deionized water (600 μL), isopropanol (350 μL), and 5% Nafion solution (50 μL) were added using a pipette, and the resulting mixture was sonicated for 5 min. Subsequently, 5 μL of the suspension was gently dropped on the surface of a GCE and naturally dried to obtain the NC@ZIF-8/GCE sensor.

Electrochemical analysis
Electrochemical tests were performed using a CHI 660E potentiostat (CH Instruments). Atypical three-electrode system consisting of a bare carbon or modified glassy

carbon electrode (GCE) as the working electrode, a platinum wire as the auxiliary electrode, and a saturated Ag/AgCl reference electrode was used.

Various electrochemical analyses were carried out on NC@ZIF-8 using chronocoulometry (CC), cyclic voltammetry (CV), and differential pulse voltammetry (DPV). The CC experiment was conducted in the voltage range of 0–0.25 V. The CV method experiment was carried out in the voltage range of 0.1–0.8 V. DPV was carried out in the voltage range of −0.2 to +1.0 V.

Material characterization

SEM (HitachiSU8220) and TEM (JEOL jeem-2100) were conducted for determining the X. The elemental composition of the material was analyzed via X-ray photoelectron spectroscopy (XPS). The specific surface area and aperture of the material were determined using a micro-chemical sorbent (BET). The elemental composition of the material was analyzed by X-ray diffraction (XRD, Bruker D8 Advance).

Results and discussion
Characterization of the materials

The morphologies of the obtained materials (hollow carbon spheres and the NC@ZIF-8 composite) were observed using TEM. Figure 2a shows that the surface of the hollow carbon sphere is very regular and does not have other structures attached.

The hollow carbon spheres are distinguishable, indicating their successful synthesis using SiO2 particles as the template. The TEM image of the NC@ZIF-8 composite (Fig. 2b) reveals that some crystals are attached to the surface of the hollow carbon spheres, and the crystals present a regular octahedral structure, which is consistent with the typical morphology of ZIF-8 crystals[11]. It can therefore be concluded that the synthesis of ZIF-8 crystals on hollow carbon spheres by the in situ growth method was successful, and the synthesized crystals grew irregularly on the surface of the hollow carbon spheres. To further investigate the crystal phase, the morphologies of the synthesized materials were characterized by SEM. The SEM image of the carbon spheres in Fig. 2c shows that the surface of the hollow carbon sphere is covered with crystals, and the crystals are evenly distributed, not only on the surface of the hollow carbon sphere but also inside it. This is because some of the spheres cracked during the synthesis, and the ZIF-8 crystals were adhered to the inner walls of such spheres. Figure 2d reveals that the silica particle template used to synthesize the carbon sphere was completely etched by sodium hydroxide, resulting in a uniform hollow carbon sphere with aneat surface, which corresponds to the TEM results. These SEM results are in good agreement with the TEM results.

Figure 3 shows the XRD pattern of the NC@ZIF-8 composite, in which the peaks observed at $2\theta = 7.29$, 10.34, 12.69, 14.66, 16.38, and 17.99 are attributable to the (001), (002), (112), (022), (013), and (222) planes of the ZIF-8 crystal, respectively. This is an apparent match for ZIF-8 PDF#37-1560 and PDF#35-1981. These peaks indicate the successful formation of the MOF crystals on
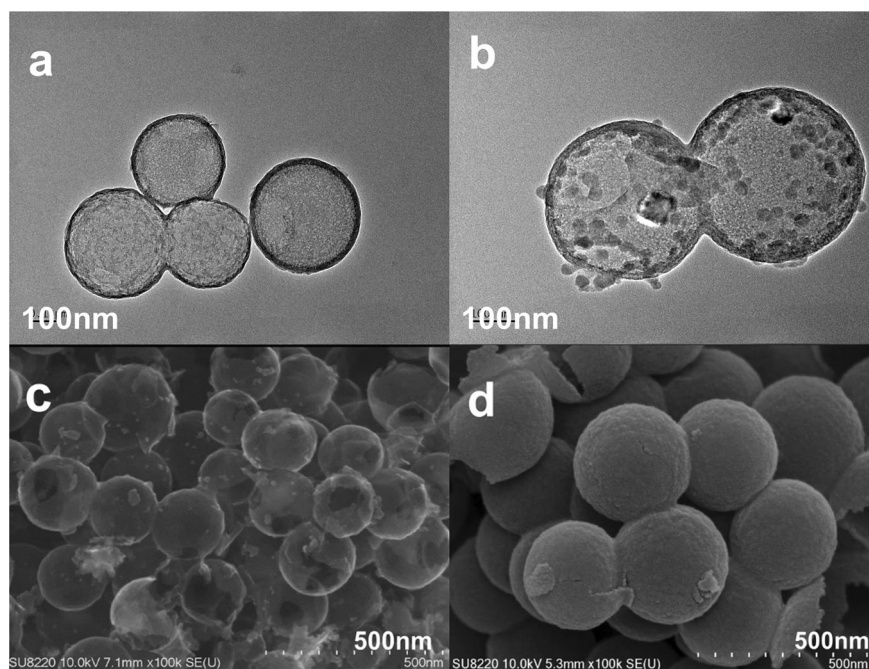

Fig. 1 The preparation process of NC@ZIF-8/GCE and the assembly of its sensor.
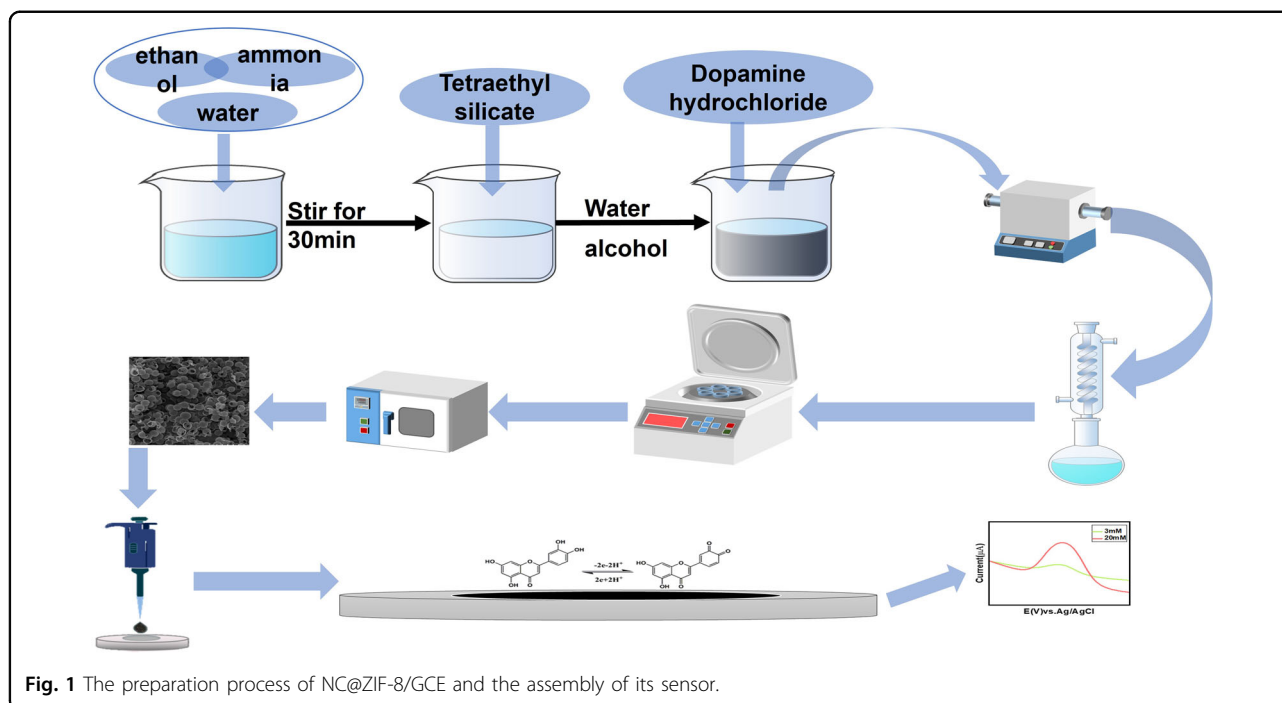
Fig. 2 Electron microscope image of NC@ZIF-8. TEM images of **a** hollow carbon spheres and **b** the NC@ZIF-8 composite. SEM images of **c** the NC@ZIF-8 composite and **d** hollow carbon spheres.
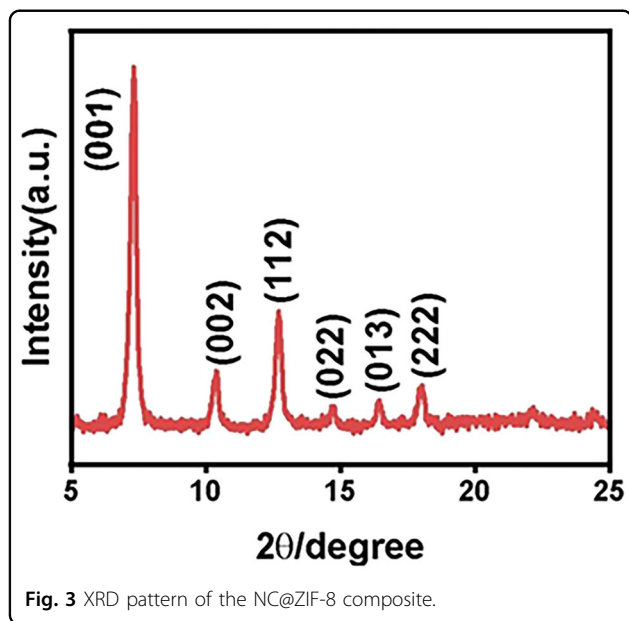

Fig. 3 XRD pattern of the NC@ZIF-8 composite.

the hollow carbon sphere[12]. However, the diffraction peaks of the hollow carbon sphere were not observed in the XRD pattern, probably because of their relatively low peak intensity compared with that of the ZIF-8 crystal peaks, which caused the diffraction peak of the hollow carbon sphere to be hidden. The XRD pattern of the NC@ZIF-8 composite is consistent with that of the

standard card, indicating that the desired material was successfully produced[13].

The functional groups of the NC@ZIF-8 composites were analyzed using X-ray photoelectron spectroscopy (XPS). As shown in Fig. 4a, the composite contains four elements: C, N, O, and Zn. Figure 4b shows that the C1s peak can be deconvoluted into five characteristic peaks at 284.6, 285.4, 286.6, 287.8, and 289 eV, corresponding to C=C, C-N, C-O, C=O, and O-C=O linkages[14]. Figure 4c shows that the O1speak can bedeconvoluted into three peaks that represent C=O, C-OH, and C-O[15] bonds at 531.4, 532.3, and 533.4 eV, respectively. Figure 4d shows the fitting of the N1s peak with three components corresponding to pyridinic, pyrrolic, and graphitic N atoms at 398.2, 399.9, and 500.9 eV, respectively[16].

Brunauer–Emmett analysis of the composite

To determine the specific surface area and material type, the BET analysis of the nitrogen adsorption-desorption curve of the NC@ZIF-8 composite was performed (see Fig. 5a). The adsorption capacity of the material increased rapidly under low relative pressures and tended to be stable after reaching a certain pressure, but it increased again at higher pressures. Compliance with type IV isotherms indicates that the material has a mesoporous structure[17]. Through BET analysis, the specific surface area of the composite was determined to be
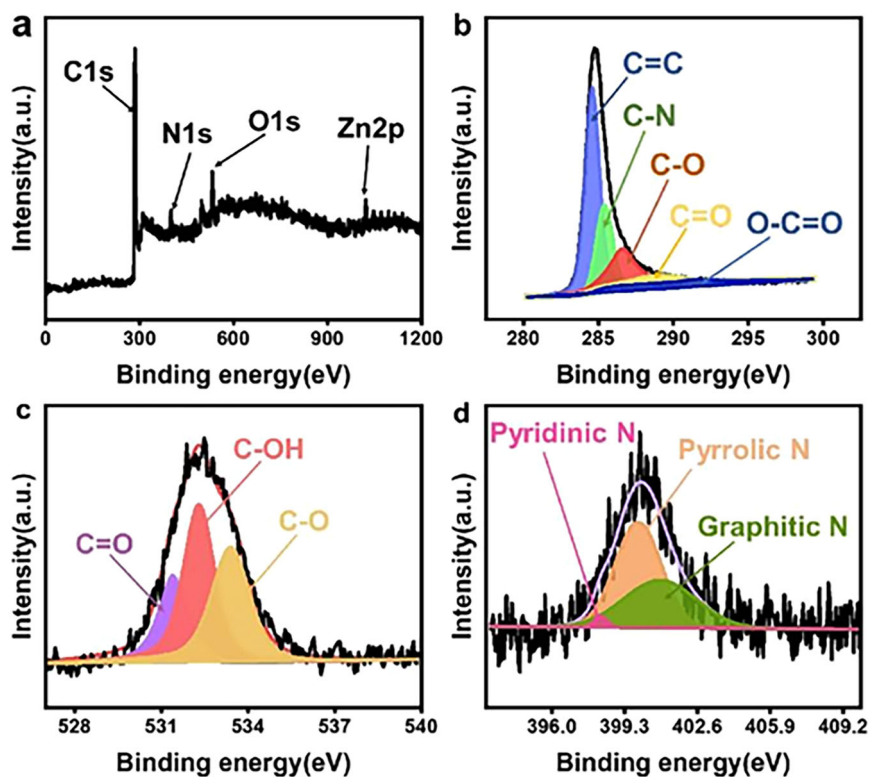
Fig. 4 XPS analysis diagram of NC@ZIF-8. a Survey XPS profile of the NC@ZIF-8 composite. **b–d** High-resolution C1s, O1s, and N1s spectra, respectively.
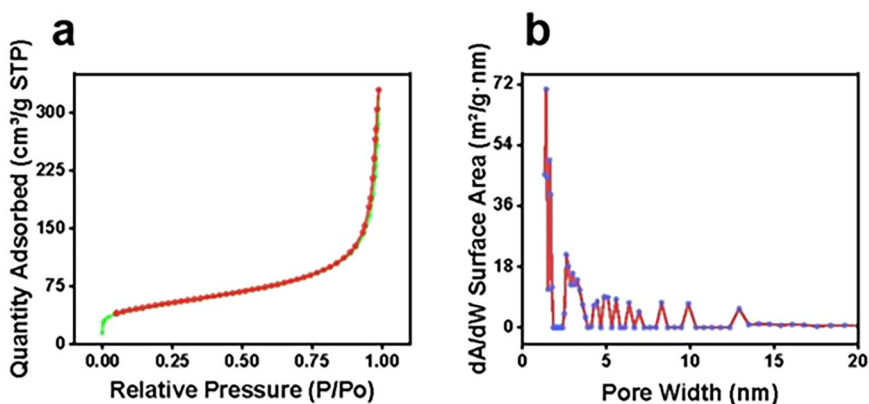

Fig. 5 BET analysis diagram of NC@ZIF-8. a Nitrogen adsorption isotherm of the NC@ZIF-8 composite. **b** Pore-size distribution.

$175.8756 \, \text{m}^2/\text{g}$. As shown in Fig. 5b, the pore size of the NC@ZIF-8 composite was mainly concentrated in the range of 2–16 nm, and the pore size range of this meso-porous material was 2–50 nm, which is consistent with the isothermal adsorption results.

Impedance analysis

The charge transfer resistance (Rct) of the modified electrode surface is characterized through electrochemical impedance spectroscopy. In general, the lower the Rct and the higher the conductivity, the smaller the curve radius, as shown in Fig. 6. The impedance of the bare electrode was the highest, while ZIF-8 exhibited significantly lower impedance, indicating improved conductivity in relation to that of the bare electrode. However, compared to NC, the composite material showed an almost linear response, suggesting the highest electron transfer rate among the tested materials.

Optimization of electrochemical conditions

For the electrochemical detection of luteolin using the NC@ZIF-8/GCE, the most important experimental parameters, such as the amount of the material used to modify the GCE, enrichment potential, enrichment time, and pH of the buffer were optimized.

Figure 7a shows the effect of the amount of NC@ZIF-8 used to modify the GCE on the peak current in DPV measurements. In DPV, the peak current is considerably
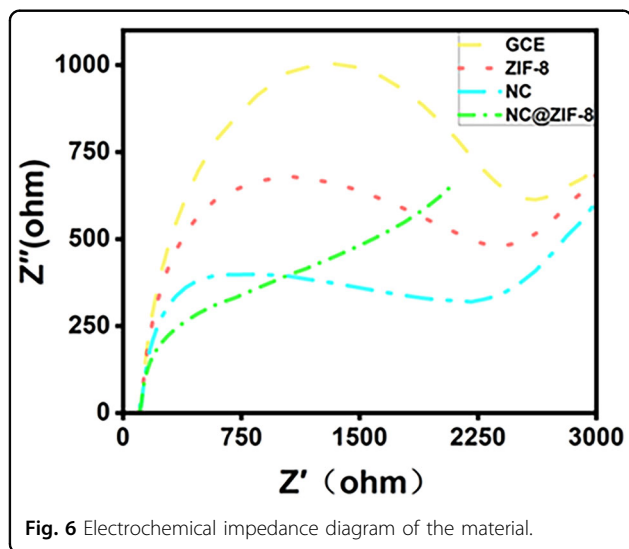
Fig. 6 Electrochemical impedance diagram of the material.

affected by the amount of the material used for GCE modification. For NC@ZIF-8/GCE, the peak current increased with the increase in the amount of NC@ZIF-8 used in GCE modification, reaching the maximum value at 3 mg/mL. However, when the amount of NC@ZIF-8 used in GCE modification was increased further, the thick layer of the composite formed on the electrode hindered electron transfer, causing the peak current to decrease. Therefore, an NC@ZIF-8 concentration of 3 mg/mL was selected as the optimal one for GCE modification.

To explore the influence of luteolin enrichment time on luteolin detection using the NC@ZIF-8/GCE, the enrichment time was varied between 60 and 180 s (the enrichment potential was fixed at 0.2 V). As shown in Fig. 7b, the enrichment time affected the peak current. As the enrichment time increased from 60 to 120 s, the peak current increased gradually. When the enrichment time reached 150 s, the electrode surface was saturated. Nevertheless, the peak current increased at a smaller rate.

Considering the comprehensive time cost and efficiency, an enrichment time of 120 s was selected for further experiments.

Figure 7c shows the effect of the enrichment potential on the peak current in the detection of luteolin using the optimized NC@ZIF-8/GCE. The enrichment potential in the range of 0.1–0.5 Vwas explored; as the enrichment potential was increased from 0 to 0.2 V, the peak current
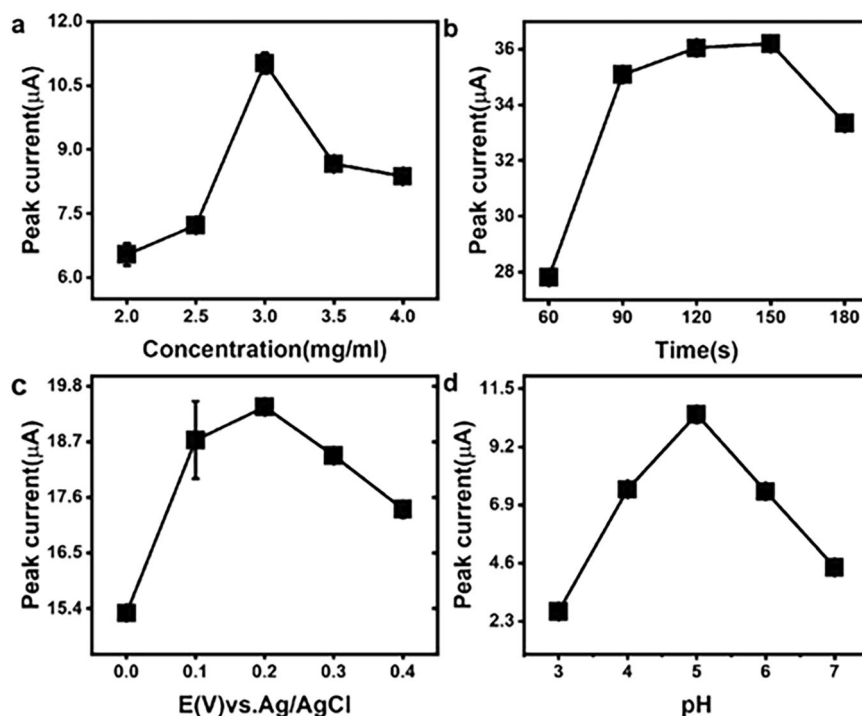
Fig. 7 NC@ZIF-8 performance optimization diagram for detecting luteolin. Effect of the **a** NC@ZIF-8 concentration used in GCE modification, **b** enrichment time, **c** enrichment potential, and **d** solution pH in the detection of 10 μM luteolin.
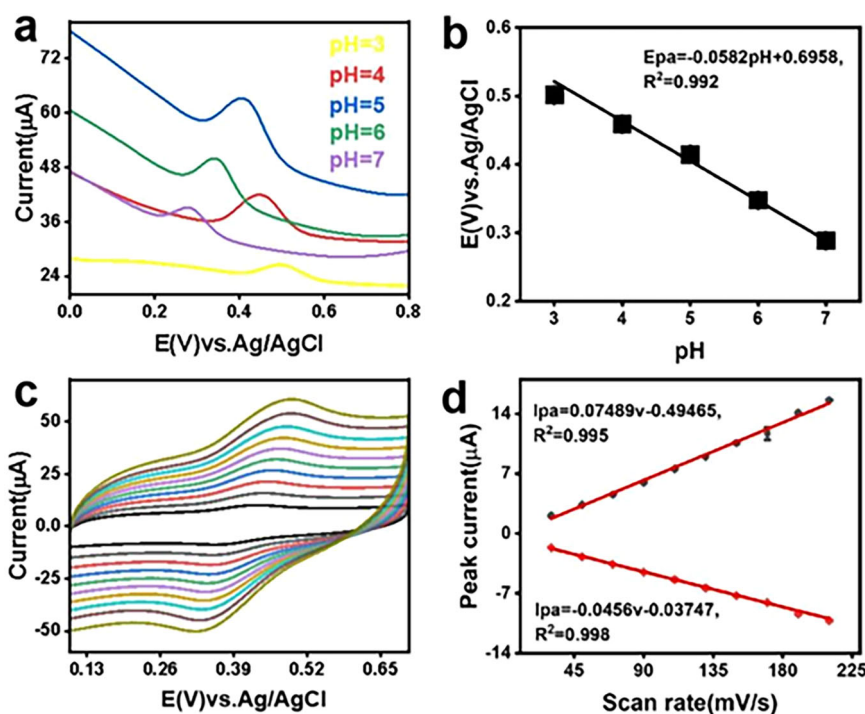
Fig. 8 Performance graph of NC@ZIF-8 under different test conditions. a DPV curve corresponding to luteolin detection at 10 µM concentration by the optimized NC@ZIF-8/GCE at different pH values, and **b** the corresponding linear relationship between the pH and applied potential. **c** CV curves of NC@ZIF-8/GCE at different scan speeds, and **d** the corresponding linear relationship between the peak current and sweep rate.

increased significantly and reached the maximum value at 0.2 V. When the enrichment potential was increased further, the peak potential decreased.

The optimal enrichment potential in this experiment was 0.2 V, and an enrichment potential of 0.2 V was used in subsequent experiments.

Next, the effect of the buffer pH on the experimental peak current was investigated. As shown in Fig. 7d, the peak current in the DPV curve increased with an increase in the buffer pH from 3 to 5, reaching the highest value at pH 5. When the buffer pH was increased further, the peak current decreased because of the decreased acidity of the solution and thus the H^+ concentration, which slowed the electron transport. Subsequent experiments were performed in a buffer solution with pH 5 to optimize the electrochemical detection of luteolin.

Effects of pH and scan rate

Figure 8a shows the DPV curves corresponding to the detection of 10 µM luteolin with an NC@ZIF-8/GCE sensor at different pH values. The solution pH strongly affected the intensity of the detected electrochemical signals. As shown in Figure 8a, Epa changed with the solution pH, and when the pH increased from 3 to 7, Epa shifted in the negative direction. As shown in Fig. 8b, the

peak potential has a good linear response relationship with pH, and the corresponding linear equation is Epa $= -0.0582$ pH $+ 0.6958$ ($R^2 = 0.992$). The slope of the line is 58.2 mV/pH, which is close to the theoretical value of 59 mV/pH based on the Nernst equation, indicating that the number of protons involved in the reaction is equal to the number of electrons transferred in the reaction[18].

To explore the redox reaction mechanism of luteolin, the electron transfer number of the reaction was calculated as 2.3 RT/nF, where R is the gas constant, T is the temperature, F is the Faraday constant, and n is the number of transferred electrons.

The electron transfer number calculated based on the peak potential difference in Fig. 8b is $n = 1.87$, which is close to 2[19].

To further study the electrochemical behavior (redox reaction) of luteolin on the NC@ZIF-8/GCE sensor, the effects of different sweep velocities in the range of 30–210 mV/s on the electrochemical peak current were studied by CV. As shown in Fig. 8c, the oxidation and reduction peak currents corresponding to the redox reaction of luteolin showed a good positive trend with scan rate v. This trend indicates that the electrochemical behavior of luteolin on the NC@ZIF-8/GCE sensor is mainly controlled by the adsorption process[20]. Figure 8d
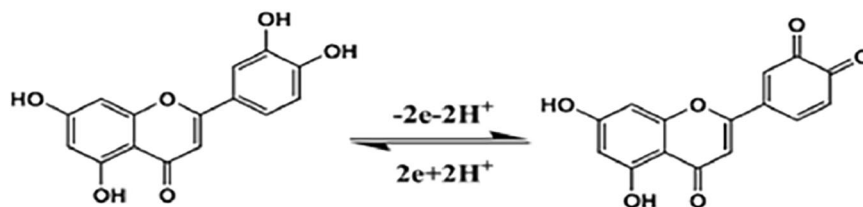
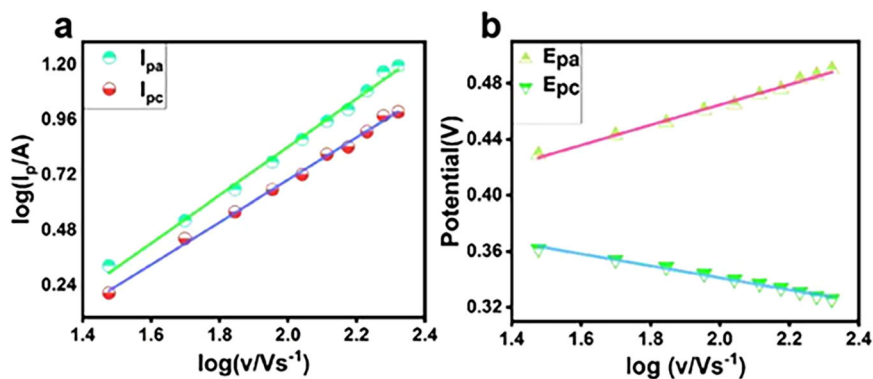**Fig. 9** Schematic of the redox reaction of luteolin on the NC@ZIF-8/GCE sensor.

Fig. 10 Potential and voltage plots of NC@ZIF-8 at different sweep rates. a The logarithmic relationship between the peak current and the scan speed; **b** the relationship curve between the logarithm of the peak current and the electric potential.

shows the linear relationship between scan rate v and oxidation peak current, and the linear equation is Ipa (Ipa $= 0.07489\,v - 0.49465$ ($R^2 = 0.995$)). Similarly, a good linear relationship between the scan rate and reduction peak current was observed, and the linear equation is Ipa $= -0.0456\,v - 0.03747$ ($R^2 = 0.998$).These results indicate that luteolin is involved in the transfer of two protons and electrons in the redox reaction during the electrochemical reaction on the NC@ZIF-8/GCE sensor, and the corresponding electrochemical reaction is shown in Fig. 9[21].

To further verify the electrochemical behavior and electron transfer number of luteolin, the slope was calculated from the relationship between peak current and the logarithm of the scan rate. If the slope is ~0.5, the reaction is diffusion-controlled; if it approaches 1, the reaction is adsorption-controlled. From the relationship graph in Fig. 10a, it can be calculated that $\log(I$pa$) = 1.047\log(v) - 1.254$, $\log(I$pc$) = 0.922\log(v) - 1.144$. The corresponding slopes are 1.047 and 0.922, both close to 1[22], indicating that the reaction is adsorption-controlled. To obtain the electron transfer number (n) of this reaction, the relationship between log v and E (V) was considered, as shown in Fig. 10b, with equations Epa $= 0.0723\log v + 0.3201$ ($R^2 = 0.992$); Epc $= -0.0429\log v + 0.4269$ ($R^2 = 0.992$). Combining with the Laviron equation[23,24], $n = 1.93$ and the charge transfer number of the reaction is 2.

Electrochemical behavior of luteolin on different electrodes

Figure 11c shows the CV curves of the bare GCE and three modified electrodes, viz., hollow carbon sphere/GCE, ZIF-8/GCE, and NC@ZIF-8/GCE. As shown, the NC@ZIF-8/GCE has the largest redox peak, indicating that its electrochemical performance is better than those of the bare electrode and the other two electrodes modified with the components of the composite (hollow carbon spheres and ZIF-8).

To determine the effective areas of the different modified electrodes, the linear relationship between charge Q and $t^{1/2}$ was obtained by evaluating the bare GCE and three differently modified electrodes by the CC method (see Fig. 11a, b). The effective areas (A) of the four different electrodes were calculated using the Anson equation[25]:

$$Q = 2nFAcD^{1/2}t^{1/2}/\Pi^{1/2} + Q_{dl} + Q_{ads} \qquad (1)$$

Here, F is the Faraday constant (96500 C/mol), c is the substrate concentration, which is 5×10^{-6} mol/cm^3, D is the standard diffusion coefficient, for which a value of 7.6×10^{-6} cm^2/s was used, Qdl isthe double-layer charge, Qads is the Faraday charge, and n is the number of electrons transferred, which was calculated to be 2. Therefore, according to Eq. (1), the active surface areas of
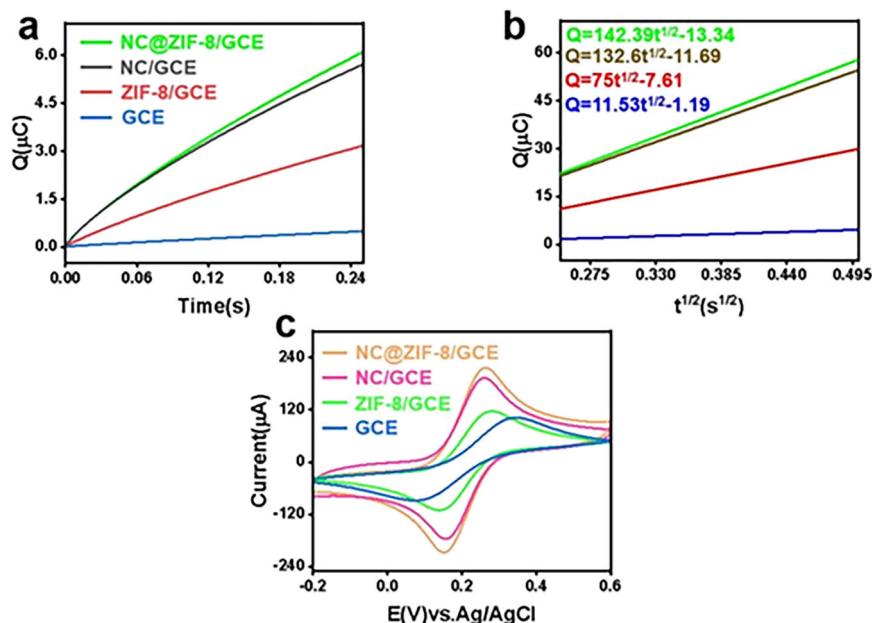
Fig. 11 Electrochemical active area and performance diagrams of different materials. a $Q–t$ curves and **b** the corresponding $Q–t^{1/2}$ plots obtained in a 5 mM $[Fe(CN)_6]^{3-/4-}$ solution. **c** CV curves of the GCE, NC/GCE, ZIF-8/GCE, NC@ZIF-8/GCE in 5 mM $[Fe(CN)_6]^{3-/4-}$ solutions containing 0.1 M KCl.

GCE, NC/GCE, ZIF-8/GCE, and NC@ZIF-8/GCE are 0.0072, 0.0472, 0.0910, and 0.0943 cm^2, respectively. Thus, the effective area of the NC@ZIF-8/GCE electrode is significantly larger than those of the other three electrodes, which is more conducive to the enrichment of luteolin.

Establishment of standard curves

After the optimization experiments, a standard curve was plotted to verify the performance of the composite sensor toward luteolin detection via DPV electroanalysis under optimized conditions. As shown in Fig. 12a, in the DPV experiment, Ipa increased as the luteolin concentration increased from 0.05 to 30 μM. As shown in Fig. 12b, Ipa exhibited a good linear relationship with the concentration of luteolin (c), and the linear equation is Ipa (μA) $= 0.98847$ c (μM) $+ 0.92779$, $R^2 = 0.998$. The NC@ZIF-8/GCE sensor had a limit of detection (LOD, S/N $= 3$) of 0.011 μM for luteolin. The experimental results indicate that as-prepared NC@ZIF-8/GCE has a broad linear concentration range and low LOD, making it suitable for specific practical applications. As shown in Fig. 12c, Ipa increased as the luteolin concentration increased from 1 to 20 mM, indicating that NC specifically detects luteolin. For Ipa and current, as shown in Fig. 12d, the linear equation is Ipa $= 0.8241$ c $+ 2.15789$ and $R^2 = 0.998$. As shown in Fig. 12e, ZIF-8 specifically detects luteolin, with the Ipa in DPV increasing as the

luteolin concentration increased from 3 to 12 mM. For Ipa and current, as shown in Fig. 12f, the linear equation is Ipa $= 4.41722$ c $+ 0.9628$, $R^2 = 0.993$. Comparing the standard curves of the three materials, NC@ZIF-8 was found to be the most effective for the specific detection of luteolin.

Repeatability and reproducibility testing of the NC@ZIF-8/GCE

The repeatability and reproducibility of the NC@ZIF-8/GCE sensor were evaluated by conducting DPV under the optimized conditions (Fig. 13). To study the repeatability of the electrode, a freshly prepared NC@ZIF-8/GCE was used in the detection of 10 μM luteolin up to 8 times. To study the reproducibility of the NC@ZIF-8/GCE sensor, eight replicate NC@ZIF-8/GCE sensors were prepared to detect luteolin at 10 μM concentration. The relative standard deviations (RSDs) for repeatability and reproducibility are 2.62 and 1.26%, respectively. These results reveal that the NC@ZIF-8/GCE sensor has good repeatability and reproducibility, and thus has good application potential.

Anti-interference capability of NC@ZIF-8/GCE in luteolin detection

Under the optimized experimental conditions, the anti-interference ability of the NC@ZIF-8 composite in luteolin detection was evaluated by DPV. K+, Cl$^-$, Mg^{2+}, Na+, and NO3$^-$ were added at 500-fold; at 100-fold,
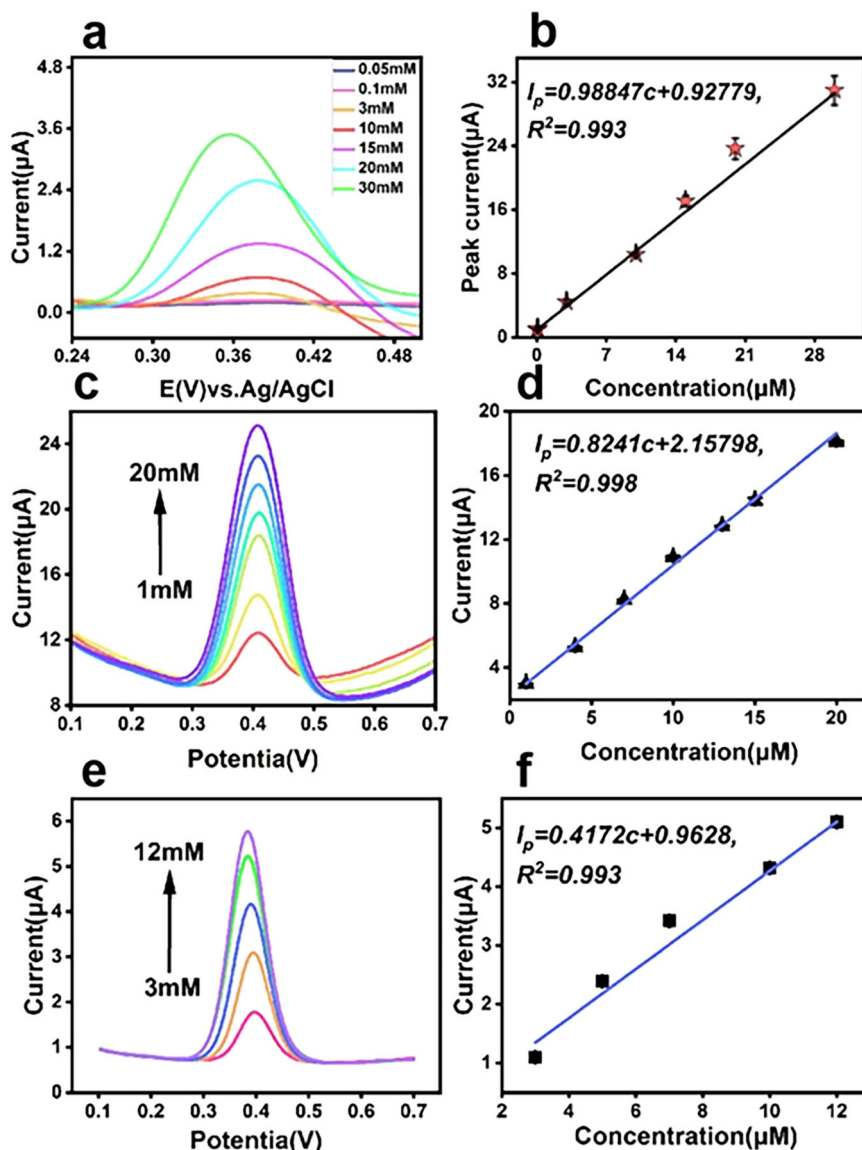
Fig. 12 Shows the detection effect of luteolin by different materials. a DPV curves of the NC@ZIF-8/GCE electrochemical sensor at different concentrations of luteolin, and **b** the linear relationship between the luteolin concentration and peak current; **c**, **d** is the detection and standard curve of NC luteolin; **e**, **f** is the detection and standard curve of NC luteolin.

apigenin and kaempferol were added. Moreover, glucose, fructose, ascorbic acid, mannitol, and citric acid were added at 300-fold to a PBS buffer solution containing 10 μM luteolin (0.1 M), and DPV was conducted under the optimized conditions. As shown in Fig. 14, compared with the blank control group without interfering substances, the change range of the peak current for the solutions added with various interfering species was <5%, which is within the normal range. This experimental result demonstrates that these ions and substances did not interfere with luteolin detection. Therefore, the NC@ZIF-8/GCE chemical sensor can be used for the accurate, reliable, and safe detection of luteolin in actual samples.

Long-term stability

The long-term stability of composite materials is one of the important indicators to assess their quality. As shown in Fig. 15, to explore the long-term stability energy of NC@ZIF-8, the specificity detection of luteolin was conducted every ten days in the air environment for 50 days. The results showed that the specificity detection of NC@ZIF-8 in 50 days was <5%, indicating that high stability of the material over extended periods.
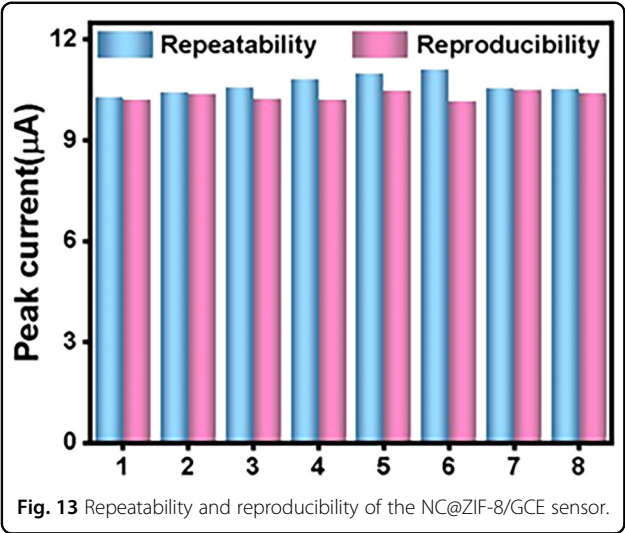
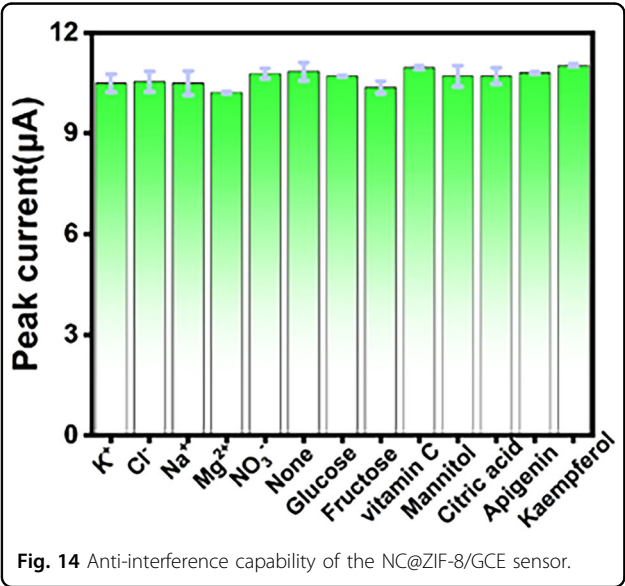**Fig. 13** Repeatability and reproducibility of the NC@ZIF-8/GCE sensor.

Fig. 15 Long-term of stability of NC@ZIF-8/GCE; data shown for 50 days.

Fig. 14 Anti-interference capability of the NC@ZIF-8/GCE sensor.

Table 1   Detection of luteolin in watermelon juice and honeysuckle extract using the NC@ZIF-8/GCE sensor.

Sample	Added (μM)	Found ± SD by DPV (μM)	Recovery (%)
Watermelon juice	0	–	–
	3	3.036 ± 0.146	101.22
	10	9.809 ± 0.261	98.09
	20	19.903 ± 0.750	99.52
Honeysuckle	0	1.338 ± 0.066	–
	3	4.139 ± 0.066	95.41
	10	11.086 ± 0.228	97.78
	20	21.351 ± 0.297	100.06

Detection of actual samples

To evaluate the ability of the NC@ZIF-8/GCE sensor to detect luteolin in actual samples, a standard addition method was used for its detection in honeysuckle extract and watermelon juice. Honeysuckle was purchased from a local pharmacy, and watermelons were obtained from a local supermarket. For extraction, 1 g of honeysuckle was suspended in 10 mL of absolute ethanol, the mixture was sonicated for 1 h, and the filtrate was collected. The volume of the test sample was then made up with ethanol solution in a 100 mL volumetric flask. The watermelon was manually squeezed into watermelon juice and filtered, and the clear filtrate was diluted 100 times with aqueous ethanol. The results are shown in the Table 1, the recovery rate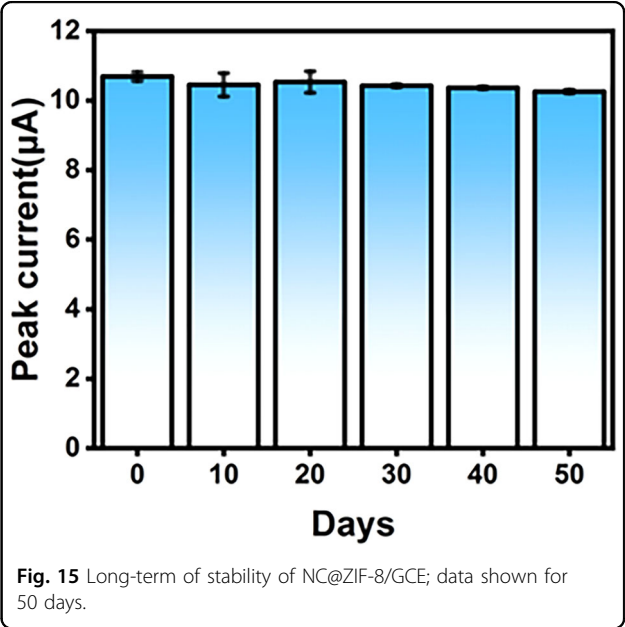s of luteolin in honeysuckle extract and watermelon juice samples were 95.41–100.06% and 98.09–101.20%, respectively. These results prove that the NC@ZIF-8/GCE chemical sensor can effectively detect luteolin in actual samples. Thus, the NC@ZIF-8/GCE chemical sensor can be used accurately, reliably, and safely to detect luteolin in actual samples.

Conclusion

ZIF-8 was synthesized on hollow carbon spheres using the original growth method to form an NC@ZIF-8 composite, which was then characterized by SEM, TEM, BET, XPS, XRD, and various electrochemical techniques, such as CV, DPV, and CC. Comprehensive structural characterization using various techniques indicated that the composite was successfully produced. The specific surface

area of the hollow carbon sphere was significantly increased after the formation of ZIF-8 crystals on its surface, and more active sites were added to enhance its electrochemical catalytic activity. The NC@ZIF-8 composite's outstanding performance in detecting luteolin in analytical samples was further verified. In addition, its excellent performance in the presence of interfering agents and good stability in terms of repeatability and reproducibility were verified. The NC@ZIF-8 sensor exhibited a good linear range and a low LOD in luteolin detection. Finally, the NC@ZIF-8 sensor achieved good recovery in the detection of luteolin in watermelon juice and honeysuckle extract. Thus, the sensor developed in this study is expected to be an ideal candidate for determining luteolin in real samples.

Author details
[1]Guangxi Key Laboratory of Green Processing of Sugar Resources, College of Biological and Chemical Engineering, Guangxi-University of Science and-Technology, Liuzhou, Guangxi, PR China. [2]GRG Metrology & Test (Nanning) Co., Ltd, Nanning, Guangxi, PR China. [3] School of Medicine, Guangxi University of Science and Technology, Liuzhou, China. [4]Province and-Ministry Co-sponsored Collaborative Innovation Center of Sugarcane and SugarIndustry, Nanning, Guangxi, PR China

Author contributions
Guosheng Liang: Method development, data acquisition analysis, writing-original draft; Yan Xiao: Data curation, analysis; Qiaoling Jing: data analysis; Tingfan Tang: Resources, supervision, editing; Jun Feng: Analysis, main review, supervision; Hao Cheng: Method development, validation, and funding acquisition.

Data availability
Data will be made available on request.

Competing interests
The authors declare no competing interests.

Publisher's note
Springer Nature remains neutral with regard to jurisdictional claims in published maps and institutional affiliations.

References
1. Zhang, L. et al. Rapid quantitative detection of luteolin using an electrochemical sensor based on electrospinning of carbon nanofibers doped with single-walled carbon nanoangles. *Anal. Methods* **15**, 3073–3083 (2023).
2. Richard, S. et al. Solubility of luteolin and other polyphenolic compounds in water, nonpolar, 401 polar aprotic and protic solvents by applying FTIR/HPLC. *Processes* **9**, 402 (2021).
3. Skoko, S., Ambrosetti, M., Giovannini, T. & Cappelli, C. Simulating absorption spectra of flavonoids in aqueous solution: a polarizable QM/MM study. *Molecules* **25**, 5853 (2020).
4. Wang, S.-P. & Huang, K.-J. Determination of flavonoids by high-performance liquid chromatography and capillary electrophoresis. *J. Chromatogr. A* **1032**, 273–279 (2004).
5. Gao, F. et al. NiO@Ni-MOF nanoarrays modified Ti mesh as an ultrasensitive electrochemical sensing platform for luteolin detection. *Talanta* **215**, 120891 (2020).
6. Zhang, Y. et al. Luminescent sensors based on metal-organic frameworks. *Coord. Chem. Rev.* **354**, 28–45 (2018).
7. Li, Y. et al. Bimetallic PdCu anchored to 3D flower-like carbon material for portable and efficient detection of glyphosate. *J. Hazard. Mater.* **480**, 135786 (2024).
8. Dai, H. et al. Recent advances on ZIF-8 composites for adsorption and photocatalytic wastewater pollutant removal: fabrication, applications and perspective. *Coordination Chem. Rev.* **441**, https://doi.org/10.1016/j.ccr.2021.213985 (2021).
9. Li, J. et al. Ultrasensitive electrochemical sensor for fenitrothion based on MIL-125 derived iron/titanium bimetallic oxides doped porous carbon composite. *Microchem. J.* **200**, 110426 (2024).
10. Liu, C. et al. Controllable synthesis of N-doped hollow-structured mesoporous carbon spheres by an amine-induced Stöber-silica/carbon assembly process. *J. Mater. Chem. A* **4**, 11916–11923 (2016).
11. Zheng, G. et al. Shape control in ZIF-8 nanocrystals and metal nanoparticles@ZIF-8 heterostructures. *Nanoscale* **9**, 16645–16651 (2017).
12. Seoane, B., Zamaro, J. M., Tellez, C., Coronas, J. Sonocrystallization of zeolitic imidazolate frameworks (ZIF-7, ZIF-8, ZIF-11, and ZIF-20). *CrystEngComm*, **14**, https://doi.org/10.1039/c2ce06382d (2012).
13. Jin, Y. -f. et al. A sensitive electrochemical sensor based on ZIF-8–acetylene black–chitosan nanocomposites for rutin detection. *RSC Adv.* **8**, 32740–32746 (2018).
14. Lakshmanakumar, M. et al. Fabrication of GQD-electrodeposited screen-printed carbon electrodes for the detection of the CRP biomarker. *ACS Omega* **6**, 32528–32536 (2021).
15. Wang, C. et al. Efficient removal of uranium(VI) from aqueous solutions by triethylenetetramine-functionalized single-walled carbon nanohorns. *ACS Omega* **5**, 27789–27799 (2020).
16. Dutta, K. et al. Development of an efficient immunosensing platform by exploring single-walled carbon nanohorns (SWCNHs) and nitrogen-doped graphene quantum dot (N-GQD) nanocomposite for early detection of cancer biomarker. *ACS Biomater. Sci. Eng.* **7**, 5541–5554 (2021).
17. Baldovino-Medrano, V. G., Niño-Celis, V. & Isaacs Giraldo, R. Systematic analysis of the nitrogen adsorption–desorption isotherms recorded for a series of materials based on microporous–mesoporous amorphous aluminosilicates using classical methods. *J. Chem. Eng. Data* **68**, 2512–2528 (2023).
18. Kumar, A. et al. Amperometric microsensor based on nanoporous gold for ascorbic acid detection in highly acidic biological extracts. *Anal. Chim. Acta* **1095**, 61–70 (2020).
19. Xie, Y., Zhang, T., Chen, Y., Wang, Y. & Wang, L. Fabrication of core-shell magnetic covalent organic frameworks composites and their application for highly sensitive detection of luteolin. *Talanta* **213**, 120843 (2020).
20. Supchocksoonthorn, P., Alvior Sinoy, M. C., deLuna, M. D. G. & Paoprasert, P. Facile fabrication of 17β-estradiol electrochemical sensor using polyaniline/carbon dot-coated glassy carbon electrode with synergistically enhanced electrochemical stability. *Talanta* **235**, 122782 (2021).
21. Cheng, H. et al. Facile synthesis of Co9S8 nanocages as an electrochemical sensor for luteolin detection. *J. Electrochem. Soc.* **168**, https://doi.org/10.1149/19457111/ac1813 (2021).
22. Li, Y. et al. An ultrasensitive dietary caffeic acid electrochemical sensor based on Pd-Ru bimetal catalyst doped nano sponge-like carbon. *Food Chem.* **425**, 136484 (2023).
23. Li, Y. et al. Ultrasensitive luteolin electrochemical sensor based on novel lamellar CuZn@ nitrogen-containing carbon nanosheets. *Nanomaterials* **13**, 171 (2022).
24. Li, J. et al. Detection of luteolin in food using a novel electrochemical sensor based on cobalt-doped microporous/mesoporous carbon encapsulated peanut-like FeOx composite. *FoodChemistry* **435**, 137651 (2024).
25. Zhang, H., Xing, Z., Pan, M., Wang, H.-B. & Liu, Y.-M. Highly sensitive and selective electrochemical determination of 4-aminophenol based on flower-like Ag-Au nanocomposites modified glassy carbon electrode. *J. Electrochem. Soc.* **167**, 12 (2020).